

Detection of Pd(III) and Pd(IV) Intermediates during the Aerobic Oxidative C–C Bond Formation from a Pd(II) Dimethyl Complex

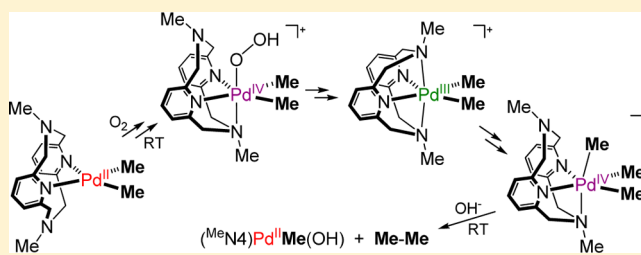
Fengzhi Tang,[†] Ying Zhang,[†] Nigam P. Rath,[‡] and Liviu M. Mirica^{*,†}

[†]Department of Chemistry, Washington University, One Brookings Drive, St. Louis, Missouri 63130-4899, United States

[‡]Department of Chemistry and Biochemistry, University of Missouri–St. Louis, One University Boulevard, St. Louis, Missouri 63121-4400, United States

Supporting Information

ABSTRACT: The dimethyl Pd^{II} complex (^{Me}N4)Pd^{II}Me₂ (^{Me}N4 = *N,N'*-dimethyl-2,11-diaza[3,3](2,6)pyridinophane) is readily oxidized by dioxygen in the presence of protic solvents to selectively eliminate ethane. UV–vis, EPR, ESI-MS, and NMR studies reveal the formation of several Pd^{III} and Pd^{IV} intermediates during the aerobically induced C–C bond formation reaction, including the key intermediate [(κ^3 -^{Me}N4)-Pd^{IV}Me₃]⁺, which leads to ethane elimination. The latter complex was also synthesized independently and structurally characterized to reveal a distorted octahedral geometry that is proposed to promote facile reductive elimination. Overall, this study represents a rare example of aerobic oxidation of an organometallic Pd^{II} precursor that leads to a well-defined Pd^{IV} species, which undergoes selective C–C bond formation under ambient conditions.



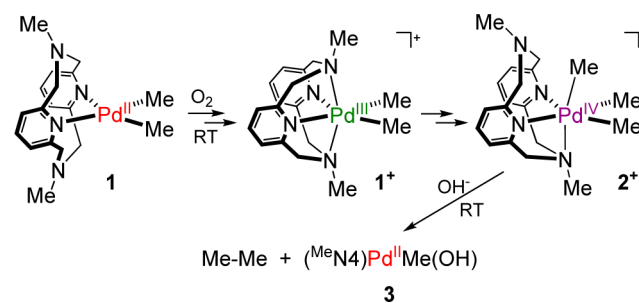
INTRODUCTION

The recent development of Pd-catalyzed aerobic transformations provides a promising and practical use of dioxygen (O₂) as an environmentally friendly and cheap oxidant in a variety of oxidative organic transformations.¹ Most of the reported reactions involve Pd^{0/II} catalytic cycles in which O₂ acts as the terminal oxidant to regenerate the Pd^{II} species.¹ In addition, high-valent Pd^{IV} and/or Pd^{III} species have been recently proposed as active intermediates in several catalytic and stoichiometric aerobic transformations.² However, the detection of such Pd^{III} or Pd^{IV} intermediates has been reported only in a very limited number of cases.^{3–5} In this regard, use of a ligand system that can stabilize both Pd^{III} and Pd^{IV} complexes and promote aerobic oxidation of organometallic Pd^{II} precursors can provide key insight into the mechanisms of these important aerobic transformations, as well as enable the development of new Pd-catalyzed aerobic transformations.

We have recently reported that the dimethyl complex (^{tBu}N4)Pd^{II}Me₂ (^{tBu}N4 = *N,N'*-di-*tert*-butyl-2,11-diaza[3,3](2,6)pyridinophane) is oxidized by O₂ and leads to selective elimination of ethane from the Pd^{III} intermediate [(^{tBu}N4)-Pd^{III}Me₂]⁺.⁴ Although several Pd^{IV} species were proposed as transient intermediates in that case, they were not observed experimentally. In addition, the formation of a Pd^{IV} species [(Me₃tacn)Pd^{IV}Me₃]⁺ was observed upon the aerobic oxidation of (Me₃tacn)Pd^{II}Me₂ (Me₃tacn = *N,N,N'*-trimethyl-1,4,7-triazacyclononane).⁵ However, in the latter case the Pd^{IV} species eliminates ethane only at elevated temperatures. Herein, we report the aerobic oxidation of the dimethyl complex (^{Me}N4)Pd^{II}Me₂ (**1**, ^{Me}N4 = *N,N'*-dimethyl-2,11-diaza[3,3](2,6)pyridinophane), which leads to facile and selective

formation of ethane under ambient conditions (Scheme 1). In addition, several Pd^{III} and Pd^{IV} intermediates were detected

Scheme 1. Aerobic C–C Bond Formation Reactivity of (^{Me}N4)Pd^{II}Me₂



in the reaction mixture by UV–vis, EPR, ESI-MS, and NMR, including the Pd^{IV} species [(κ^3 -^{Me}N4)Pd^{IV}Me₃]⁺, which generates ethane upon reductive elimination. The [(κ^3 -^{Me}N4)-Pd^{IV}Me₃]⁺ complex was also independently synthesized, and its C–C bond formation reactivity was investigated. Overall, this system represents a rare example of aerobic oxidation of an organometallic Pd^{II} complex to generate detectable high-valent Pd intermediates and lead to oxidative C–C bond formation reactivity. In addition, these studies provide strong evidence for the recently proposed mechanism of inner-sphere O₂ reduction

Received: August 6, 2012

Published: August 31, 2012

at a Pd^{II} center followed by C–C reductive elimination from a Pd^{IV} center.^{4,5}

EXPERIMENTAL DETAILS

General Specifications. All manipulations were carried out under a nitrogen atmosphere using standard Schlenk and glovebox techniques if not indicated otherwise. All reagents for which the synthesis is not given were commercially available from Aldrich, Acros, STREM, or Pressure Chemical and were used as received without further purification. Solvents were purified prior to use by passing through a column of activated alumina using an MBRAUN SPS. *N,N'*-Dimethyl-2,11-diaza[3,3](2,6)pyridinophane (^{Me}N4)⁶ was prepared according to the literature procedure, and (^{Me}N4)Pd^{II}Me₂ (**1**) and [(^{Me}N4)Pd^{III}Me₂]ClO₄ ([1⁺]ClO₄) were synthesized in a manner similar to the ^{tBu}N4 analogues.^{7,8} NMR spectra were obtained on a Varian Mercury-300 spectrometer (300.121 MHz) or a Varian Unity Inova-600 spectrometer (599.746 MHz). UV–vis spectra were recorded on a Varian Cary 50 Bio spectrophotometer and are reported as λ_{max}, nm (ε, M⁻¹ cm⁻¹). EPR spectra were recorded on a JEOL JES-FA X-band (9.2 GHz) EPR spectrometer at 77 or 298 K. ESI-MS experiments were performed using a Bruker Maxis Q-TOF mass spectrometer with an electrospray ionization source. Elemental analyses were carried out by the Columbia Analytical Services Tucson Laboratory. Cyclic voltammetry experiments were performed with a BASi EC Epsilon electrochemical workstation. Electrochemical grade Bu₄NClO₄ (Fluka) was used as the supporting electrolyte. Electrochemical measurements were performed under a blanket of nitrogen, and the analyzed solutions were deaerated by purging with nitrogen. A glassy carbon disk electrode and a Ag/0.01 M AgNO₃/MeCN electrode were used as the working and reference electrode, respectively. The reference electrode was calibrated against Cp₂Fe (Fc).

Synthesis of [(^{Me}N4)Pd^{IV}Me₃]⁺ ([2⁺]). Under N₂, **1** (20.1 mg, 49.6 μmol) was dissolved in 3 mL of acetone. Upon addition of 1 equiv of MeI (31 μL, 49.6 μmol), a brownish precipitate formed immediately. The reaction mixture was stirred at room temperature for about 20 min and then stored at –35 °C for 3 h. The clear yellow solution was decanted, and the brown product was washed with 2 × 1 mL of precooled acetone and dried under vacuum for 10 min. Yield: 14.6 mg, 54%. The resulting solid was dissolved in CD₃CN, and the NMR was taken immediately. X-ray quality crystals were obtained from a solution in acetone at –35 °C. ¹H NMR (CD₃CN), 20 °C (δ, ppm): 7.56 (t, *J* = 7.8 Hz, 2 H, py-H), 7.08 (d, *J* = 7.8 Hz, 4 H, py-H), 4.73 (d, *J* = 15.0 Hz, 4 H, –CH₂–), 4.00 (d, *J* = 18.3 Hz, 4 H, –CH₂–), 2.65 (s, 6 H, –N–CH₃), 1.80 (s, 9H, Pd^{IV}–CH₃). ESI-MS: *m/z* 419.1420, calcd for [(^{Me}N4)Pd^{IV}Me₃]⁺ 419.1427. The elemental analysis of this complex could not be obtained due to its thermal sensitivity.

General Procedure for the Oxidation of **1 with O₂.** A 4–5 mM solution of **1** with an equimolar amount of 1,3,5-trimethoxybenzene or 1,4-dioxane (used as internal standards) was dissolved in 2.4 mL of O₂-saturated CD₃OD/C₆D₆ or D₂O/CD₃CN solution, and an NMR tube was filled to the top (to avoid the escape of volatiles into the headspace) and sealed with a septum. The reaction mixture was kept in the dark and periodically analyzed by ¹H NMR. The yields of Pd intermediates and organic/Pd products were determined by integration versus the internal standard, calculated as [moles of product]/[moles of **1**] × 100% and given as an average of two runs.

UV–Vis Studies of Oxidation of **1 with O₂.** A ~5 mM solution of **1** in 1:1 MeOH/PhH was placed into a quartz cuvette (path length 1.0 cm) equipped with a septum-sealed cap and a magnetic stir bar. Oxygen was bubbled through the solution for 2–3 min, and the reaction mixture was stirred under O₂ at 20 °C in the dark. The reaction progress was monitored by UV–vis. The concentration of 1⁺ during the reaction was calculated based on the extinction coefficient of the 620 nm absorption band (ε = 422 M⁻¹ cm⁻¹ in 1:1 MeOH/PhH). The same aerobic oxidation experiment was performed for a 5.2 mM solution of (^{Me}N4)Pd^{II}Me₂ in 5% H₂O/MeCN.

EPR Studies of Oxidation of **1 with O₂.** A 4.5 mM solution of **1** in degassed 1:1 MeOH/PhH was prepared immediately before the experiment. Oxygen was bubbled through the solution for 2 min, and the reaction mixture was left to stand in the dark for 10 min at 20 °C. The solution was then transferred to a quartz EPR tube, and the EPR spectrum was recorded at 77 K.

DMPO Spin Trapping Studies of Oxidation of **1 with O₂.** Under N₂, 250 μL of a freshly prepared 9.0 mM solution of **1** in degassed benzene was mixed with 250 μL of a freshly prepared 90 mM solution of DMPO in degassed MeOH and placed in a vial equipped with a septum ([**1**] = 4.5 mM, [DMPO] = 45 mM). O₂ was bubbled through the solution for 1 min, the solution was then transferred to an EPR tube, and the EPR spectrum was recorded immediately at 293 K.

ESI-MS Studies of Oxidation of **1 with O₂.** A 0.1 mg amount of **1** was dissolved in 1 mL of 5% H₂O/MeCN, and air or O₂ was bubbled through the solution for about 30 s. Then 50 μL of the solution was injected into the MS instrument at various time points to detect any transient intermediates present in the reaction mixture.

X-ray Structure Determination of **1 and [2⁺].** Suitable crystals were mounted on Mitgen cryoloops in random orientations in a Bruker Kappa Apex-II CCD X-ray diffractometer equipped with an Oxford Cryostream LT device and a fine focus Mo Kα radiation X-ray source (λ = 0.71073 Å). Preliminary unit cell constants were determined with a set of 36 narrow frame scans. Typical data sets consist of combinations of φ and ψ scan frames with a typical scan width of 0.5° and a counting time of 15–30 s/frame at a crystal-to-detector distance of ~4.0 cm. The collected frames were integrated using an orientation matrix determined from the narrow frame scans. Apex II and SAINT software packages⁹ were used for data collection and data integration. Analysis of the integrated data did not show any decay. Final cell constants were determined by global refinement of xyz centroids of reflections from the complete data sets. Collected data were corrected for systematic errors using SADABS⁹ based on the Laue symmetry using equivalent reflections. Structure solutions and refinement were carried out using the SHELXTL-PLUS software package.¹⁰ The structures were refined with full matrix least-squares refinement by minimizing Σw(F_o² – F_c²)². All non-hydrogen atoms were refined anisotropically to convergence, and the hydrogen atoms were added at the calculated positions in the final refinement cycles. Crystal data and intensity data collection parameters are listed in Tables S11–S14.

RESULTS AND DISCUSSION

Characterization and Aerobic Reactivity of (^{Me}N4)-Pd^{II}Me₂ (1**).** The ^{Me}N4 ligand was synthesized using a reported synthetic procedure,⁶ and the Pd^{II} precursor (^{Me}N4)Pd^{II}Me₂, **1**, was obtained in a manner similar to the ^{tBu}N4 analogue.^{4,8} The X-ray structure of **1** reveals a square-planar geometry around the Pd^{II} center with two methyl ligands and the two pyridine N atoms of the ^{Me}N4 ligand binding equatorially, while the two amine donors are pointing away from the metal center (Figure 1, left). The cyclic voltammogram of **1** in 0.1 M Bu₄NClO₄/MeCN exhibits an anodic wave at –520 mV vs Fc⁺/Fc that is assigned to a Pd^{II/III} oxidation (Figure 2), which is significantly lower than that of the reported analogue (^{tBu}N4)Pd^{II}Me₂ (–360 mV vs Fc⁺/Fc).⁴ In addition, a reversible second oxidation wave assigned to the Pd^{III/IV} oxidation is found to have an uncommonly low E_{1/2}^{III/IV} value of –400 mV vs Fc⁺/Fc.⁸ These low oxidation potentials are likely due to the ability of the ^{Me}N4 ligand to provide two additional N-donors to stabilize six-coordinate Pd^{III} and Pd^{IV} species, while the less bulky N-Me groups can accommodate the more compact structure of a Pd^{IV} center.¹¹ In light of these results, it is expected that **1** can be easily oxidized by mild oxidants to generate detectable Pd^{III} and/or Pd^{IV} species. Indeed, **1** was found to readily react with O₂ in the presence of protic solvents (i.e., MeOH/PhH or H₂O/MeCN solvent mixtures), and

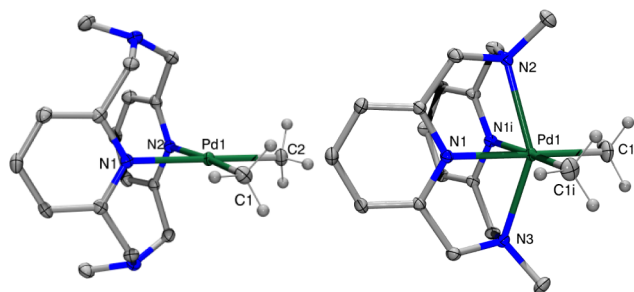


Figure 1. ORTEP representation (50% probability ellipsoids) of **1** (left) and the cation of $[1^+]ClO_4$ (right). Selected bond distances (Å) and angles (deg): **1**, Pd1–C1 2.035(2), Pd1–C2 2.037(2), Pd1–N1 2.1585(18), Pd1–N2 2.1718(18); 1^+ , Pd1–C1 2.0432(10), Pd1–C1i 2.0433(10), Pd1–N1 2.1393(7), Pd1–N1i 2.1393(7), Pd1–N2 2.4013(11), Pd1–N3 2.3506(12), N2–Pd1–N3 145.37(4). The structure of $[1^+]ClO_4$ is taken from ref 11 and is shown only for comparison.

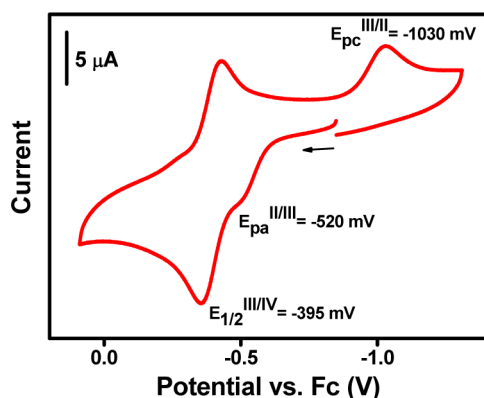
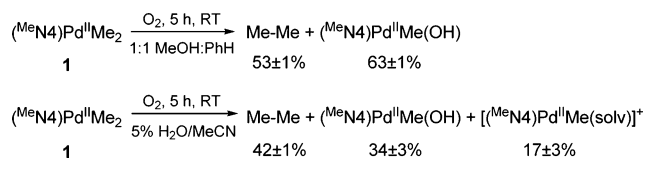


Figure 2. Cyclic voltammogram of **1** in 0.1 M $Bu_4NClO_4/MeCN$, 100 mV/s scan rate.

monitoring of the reaction by NMR shows an aerobically induced ethane formation in up to 53% yield (Scheme 2),

Scheme 2. Aerobic Reactivity of $(^{Me}N_4)Pd^{III}Me_2$ (**1**)¹²



similar to the previously reported $(^{tBu}N_4)Pd^{III}Me_2$ complex.⁴ Moreover, the observed C–C bond formation reactivity is not affected by the presence of the alkyl radical trap TEMPO,⁸ suggesting a nonradical mechanism (vide infra).

Detection of the Pd^{III} Intermediate $[(^{Me}N_4)Pd^{III}Me_2]^+$ (1^+). When a solution of **1** is exposed to O_2 or air in the presence of protic solvents, a green color develops and the UV–vis spectrum reveals absorption peaks at 620 and 490 nm that are identical to those of the independently synthesized complex $[(^{Me}N_4)Pd^{III}Me_2]ClO_4$, $[1^+]ClO_4$ (Figure 3).⁸ Moreover, the resulting solution exhibits an axial EPR spectrum identical to $[1^+]ClO_4$, with superhyperfine coupling to the two amine N atoms in both parallel and perpendicular directions (Figure 4), in line with the distorted octahedral geometry of the Pd^{III} center (Figure 1, right).¹¹ The formation of 1^+ was further confirmed by ESI-MS, which reveals a peak at m/z 404.1213

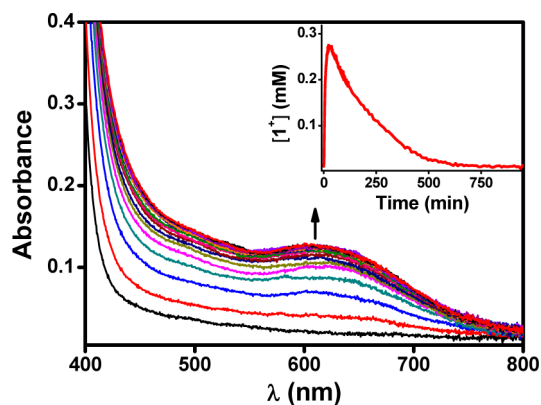


Figure 3. Formation of 1^+ during aerobic oxidation of **1** (5.2 mM) in 5% $H_2O/MeCN$ followed by UV–vis spectroscopy ($\Delta t = 2$ min, $t_{max} = 30$ min). Inset: Plot of the concentration of 1^+ during oxidation of **1** under the same conditions.

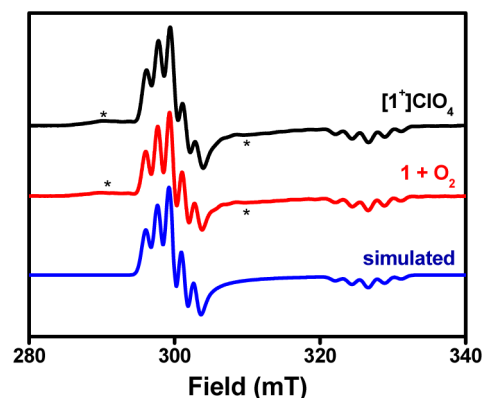


Figure 4. EPR spectra of a solution of $[1^+]ClO_4$ in 3:1 $PrCN/MeCN$ (black line), the product of oxidation of **1** with O_2 in 1:1 $MeOH/PhH$ (red line), and a simulated EPR spectrum (blue line) using the following parameters: $g_x = 2.170$ ($A_N = 16.0$ G); $g_y = 2.170$ ($A_N = 16.0$ G); $g_z = 1.990$ ($A_N = 22.5$ G). The features marked with an asterisk are due to the hyperfine coupling to the ^{105}Pd isotope ($I = 5/2$, natural abundance 22.3%).

(calcd for 1^+ : 404.1192). Interestingly, the Pd^{III} species 1^+ accumulates during the reaction up to a maximum yield of 5% in 5% $H_2O/MeCN$ and 12% in 1:1 $MeOH/PhH$, respectively. Moreover, 1^+ decays as ethane is formed, suggesting the involvement of this species as a transient intermediate in the aerobic oxidation of **1**.⁴ To confirm the role of 1^+ in ethane formation, we investigated the reactivity of the independently synthesized $[1^+]ClO_4$. While 1^+ is stable in CD_3CN in the dark, addition of OD^- leads to rapid formation of ethane in 24% yield.⁸ Hydroxide is likely generated during aerobic oxidation as a product of O_2 reduction in the presence of protons. Furthermore, this coordinating anion can promote C–C bond formation by binding to the Pd^{III} center of 1^+ and displacing one of the axial amine groups (vide infra).⁴

Detection and Characterization of the Pd^{IV} Intermediate $[(\kappa^3\text{-}^{Me}N_4)Pd^{IV}Me_3]^+$ (2^+). When the aerobic oxidation of **1** was monitored by NMR, peaks corresponding to a transient intermediate were observed in addition to those of ethane and the Pd^{II} product(s).⁸ The NMR spectrum suggests the presence of three methyl groups attached to the Pd center, and by comparison with other reported analogous species^{5,13} we assign this intermediate as a $[(\kappa^3\text{-}^{Me}N_4)$

$\text{Pd}^{\text{IV}}\text{Me}_3]^+$ (2^+) species. During the course of the reaction, 2^+ forms in up to 34% and 10% yields in O_2 -saturated 1:1 $\text{CD}_3\text{OD}/\text{C}_6\text{D}_6$ and 5% $\text{D}_2\text{O}/\text{CD}_3\text{CN}$, respectively, and its decay correlates with ethane formation, suggesting the involvement of 2^+ in C–C bond formation.⁸ In addition, the maximum yield of 2^+ also increases with an increasing concentration of the protic solvent: from only a 6% yield of 2^+ in 1% $\text{H}_2\text{O}/\text{MeCN}$ to a 32% yield in 50% $\text{H}_2\text{O}/\text{MeCN}$, as observed by NMR.⁸ This suggests that 2^+ is the product of the aerobic oxidation of **1** in the presence of protons in solution.⁴

Species 2^+ was independently synthesized by treating **1** with MeI in MeCN or acetone, to yield the $[(\kappa^3\text{-Me}_3\text{N}_4)\text{Pd}^{\text{IV}}\text{Me}_3]^+$ ($[2^+]\text{I}$) product, which has an identical NMR spectrum to that of the Pd^{IV} intermediate observed during the aerobic oxidation of **1**.⁸ The X-ray structure of $[2^+]\text{I}$ reveals a distorted octahedral Pd^{IV} center with two Me groups in the equatorial positions, while the third methyl group replaces one of the axial N atoms of the Me_3N_4 ligand (Figure 5). The Pd–Me_{eq} distances are

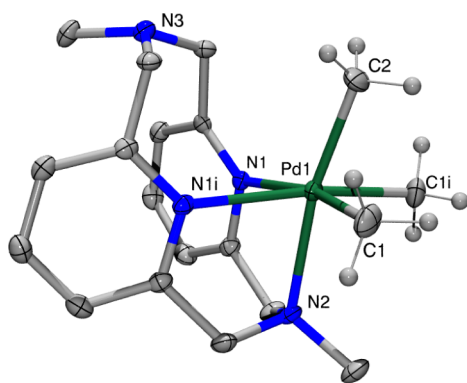
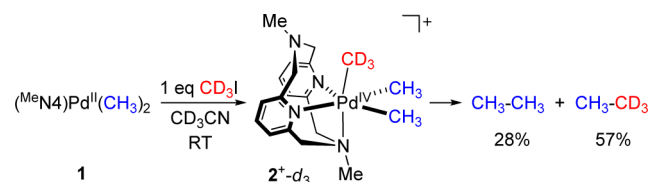


Figure 5. ORTEP representation (50% probability ellipsoids) of the cation of $[2^+]\text{I}$. Selected bond distances (Å) and angles (deg): Pd1–C1 2.035(3), Pd1–C1i 2.035(3), Pd1–C2 2.061(4), Pd1–N1 2.283(2), Pd1–N1i 2.283(2), Pd1–N2 2.231(3), N2–Pd1–C2 169.22(13), C1–Pd1–C1i 92.50(18), C1–Pd1–C2 80.62(12).

2.035 Å, similar to other reported $\text{Pd}^{\text{IV}}\text{Me}_3$ complexes,^{5,13} while the Pd–Me_{ax} distance is slightly longer (2.061 Å) and substantially tilted toward the equatorial plane, likely due to the steric clash with the adjacent methylene H atoms (Figure S14).⁸ This distortion is likely responsible for ethane elimination: while 2^+ is fairly stable at low temperatures ($t_{1/2} \approx 6.7$ days at -20°C), it easily eliminates ethane quantitatively at RT ($t_{1/2} \approx 68$ min, Figure S13). By comparison, ethane elimination from the more symmetric $[(\text{Me}_3\text{tacn})\text{Pd}^{\text{IV}}\text{Me}_3]^+$ complex is much slower and occurs only at elevated temperatures.⁵ The ^1H NMR of $[2^+]\text{I}$ in CD_3CN at RT shows one averaged singlet at 1.80 ppm corresponding to the Pd–Me H's, suggesting a rapid rearrangement of the equatorial and axial methyl groups, while two separate Pd–Me peaks are observed at -20°C in a 1:2 ratio (Figures S10, S11).⁸ The fluxionality of 2^+ was confirmed by studying the reductive elimination reactivity of $[(\kappa^3\text{-Me}_3\text{N}_4)\text{Pd}^{\text{IV}}(\text{CD}_3)(\text{CH}_3)_2]^+$ ($2^+ \text{-} d_3$), formed by reacting **1** with CD_3I in CD_3CN , which leads to formation of CH_3CH_3 and CH_3CD_3 in a 1:2 ratio,⁸ as expected for a fast rearrangement of the three methyl groups and reductive elimination of any two of the three methyl groups (Scheme 3).^{4,14}

ESI-MS Studies of the Aerobic Oxidation of 1. Electrospray mass spectrometry (ESI-MS) studies were employed to obtain additional information on the steps

Scheme 3. Reaction of **1** with CD_3I



preceding the formation of 2^+ during the aerobic oxidation of **1**. Gratifyingly, ESI-MS analysis of **1** in O_2 - or air-saturated 5% $\text{H}_2\text{O}/\text{MeCN}$ revealed several isotopic patterns that were assigned to the following cationic Pd^{III} and Pd^{IV} species: $[(^{\text{Me}}\text{N}_4)\text{Pd}^{\text{III}}\text{Me}_2]^+$ (1^+ , m/z 404.1213, calcd 404.1192), $[(^{\text{Me}}\text{N}_4)\text{Pd}^{\text{IV}}\text{Me}_3]^+$ (2^+ , m/z 419.1440, calcd 419.1429), $[(^{\text{Me}}\text{N}_4)\text{Pd}^{\text{IV}}\text{Me}_2(\text{OOH})]^+$ (4^+ , m/z 437.1196, calcd 437.1169), and $[(^{\text{Me}}\text{N}_4)\text{Pd}^{\text{IV}}\text{Me}_2(\text{OH})]^+$ (5^+ , m/z 421.1253, calcd 421.1221, Figure 6).¹⁵ These peaks were not observed

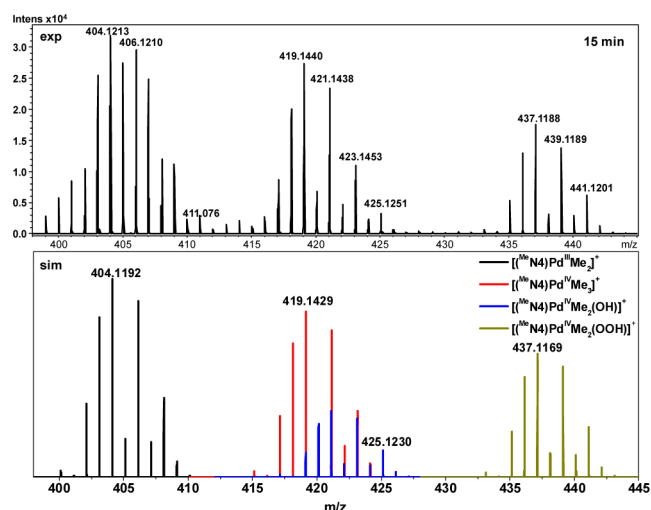


Figure 6. ESI-MS spectrum showing the isotopic pattern of cationic Pd^{III} and Pd^{IV} intermediates formed during the aerobic oxidation of **1** in 5% $\text{H}_2\text{O}/\text{MeCN}$, 15 min after exposure to air (top), and simulation of the isotopic pattern corresponding to a 1.2:1.0:0.4:0.75 ratio of $[(^{\text{Me}}\text{N}_4)\text{Pd}^{\text{III}}\text{Me}_2]^+$, $[(^{\text{Me}}\text{N}_4)\text{Pd}^{\text{IV}}\text{Me}_3]^+$, $[(^{\text{Me}}\text{N}_4)\text{Pd}^{\text{IV}}\text{Me}_2(\text{OH})]^+$, and $[(^{\text{Me}}\text{N}_4)\text{Pd}^{\text{IV}}\text{Me}_2(\text{OOH})]^+$ (bottom).

during the ESI-MS analysis of **1** in degassed MeCN or 5% $\text{H}_2\text{O}/\text{MeCN}$, suggesting that these Pd^{III} and Pd^{IV} intermediates are likely formed during the aerobic oxidation of **1** and not due to an artifact of the ESI-MS experiment. Interestingly, the relative ratio of these intermediates changes with time during the course of the aerobic oxidation. While all four species were detected at the early stages of the reaction, species 2^+ is the longest-lived intermediate (Figures S21–S24), suggesting that 1^+ , 4^+ , and 5^+ are precursors to 2^+ .⁸ In addition, the presence of 2^+ at reaction times comparable to the time scale of ethane formation further confirms its direct involvement in the reductive elimination of ethane (vide infra).

Crossover Experiments. To further probe the formation of ethane through reductive elimination from the trimethyl Pd^{IV} intermediate 2^+ , crossover experiments were performed using a 1:1 mixture of **1** and $(^{\text{Me}}\text{N}_4)\text{Pd}^{\text{II}}(\text{CD}_3)_2$, **1-}d_6. Monitoring of the aerobic oxidation reaction by NMR in O_2 -saturated 5% $\text{D}_2\text{O}/\text{CD}_3\text{CN}$ reveals formation of CH_3CH_3 and CH_3CD_3 in 14% and 15% yields, respectively. Given the typical yield of 42% ethane formed upon oxidation of **1** under similar**

($\kappa^3\text{-Me}_4\text{N}$)Pd^{III}Me₂(OH) (7) and [(Me_4N)Pd^{III}Me₂]⁺ (1⁺). The two Pd^{III} species can interconvert through displacement of one of the axial N donors of Me_4N by a hydroxide anion.^{4,18} The trimethyl Pd^{IV} species 2⁺ can then be formed by two different pathways, one of which involves a Me group transfer between the two Pd^{III} dimethyl species 1⁺ and 7. Similar Me group transfer was also reported for other Pd^{II} and Pt^{II} complexes upon one-electron oxidation.¹⁹ Another possible mechanism may involve a Pd^{IV}-to-Pd^{II} Me group transfer between 5⁺ and 1 to give 2⁺ and 3 (Scheme 5).⁴ Such methyl group transfers from electrophilic Pd^{IV}Me₃ complexes to nucleophilic Pt^{II}Me₂ or Pd^{II}Me₂ species have been observed previously.²⁰ In addition, a very similar Me group transfer reaction from a [(Me₃tacn)Pd^{IV}Me₂(OH)]⁺ to (Me₃tacn)Pd^{II}Me₂ center was recently proposed by our group.⁵

CONCLUSION

In summary, reported herein is a rare example of aerobic oxidation of an organometallic Pd^{II} precursor to form detectable Pd^{III} and Pd^{IV} species, which lead to selective C–C bond formation under ambient conditions. The detailed mechanisms of the aerobic oxidation of (Me_4N)Pd^{II}Me₂ and subsequent ethane elimination were investigated by various spectroscopic methods. UV–vis and EPR studies reveal the formation of a [(Me_4N)Pd^{III}Me₂]⁺ intermediate, and a Pd^{III}-superoxide species is proposed to form upon the initial inner-sphere oxidation of the Pd^{II} center by O₂. Interestingly, ESI-MS and NMR studies show the formation of several Pd^{IV} intermediates, including the Pd^{IV}-OOH and Pd^{IV}-OH species involved in the aerobic oxidation steps, as well as the key intermediate [(Me_4N)Pd^{IV}Me₃]⁺ responsible for ethane elimination. The latter Pd^{IV} species was also synthesized independently, and its observed ethane elimination reactivity provides unambiguous evidence for the proposed mechanism. Overall, these results strongly suggest that both Pd^{III} and Pd^{IV} oxidation states are involved in the aerobically induced C–C bond formation from a Pd^{II}Me₂ precursor: while the initial formation of a Pd^{III} species is likely necessary for an efficient aerobic oxidation, the formation of a Pd^{IV} intermediate is required for a selective and facile C–C bond formation step. Current research efforts are aimed at using the Me_4N ligand system for catalytic aerobic C–C and C–heteroatom bond formation reactions.

ASSOCIATED CONTENT

Supporting Information

Detailed experimental details, spectroscopic characterization, aerobic oxidation studies, and X-ray crystallographic data. This material is available free of charge via the Internet at <http://pubs.acs.org>.

AUTHOR INFORMATION

Corresponding Author

*E-mail: mirica@wustl.edu.

Notes

The authors declare no competing financial interest.

ACKNOWLEDGMENTS

We thank the Department of Chemistry at Washington University for startup funds, and the American Chemical Society Petroleum Research Fund (49914-DNI3) and DOE Catalysis Science Program (DE-FG02-11ER16254) for support.

We also thank Dr. Julia R. Khusnutdinova for experimental assistance. L.M.M. is a Sloan Fellow.

REFERENCES

- (1) (a) Stoltz, B. M. *Chem. Lett.* **2004**, 33, 362. (b) Stahl, S. S. *Angew. Chem., Int. Ed.* **2004**, 43, 3400. (c) Stahl, S. S. *Science* **2005**, 309, 1824. (d) Beck, E. M.; Grimster, N. P.; Hatley, R.; Gaunt, M. J. *J. Am. Chem. Soc.* **2006**, 128, 2528. (e) Sigman, M. S.; Jensen, D. R. *Acc. Chem. Res.* **2006**, 39, 221. (f) Gligorich, K. M.; Sigman, M. S. *Chem. Commun.* **2009**, 3854. (g) Campbell, A. N.; Stahl, S. S. *Acc. Chem. Res.* **2012**, 45, 851. (h) Shi, Z.; Zhang, C.; Tang, C.; Jiao, N. *Chem. Soc. Rev.* **2012**, 41, 3381.
- (2) (a) Zhang, J.; Khaskin, E.; Anderson, N. P.; Zavalij, P. Y.; Vedernikov, A. N. *Chem. Commun.* **2008**, 3625. (b) Zhang, Y.-H.; Yu, J.-Q. *J. Am. Chem. Soc.* **2009**, 131, 14654. (c) Wang, A.; Jiang, H.; Chen, H. *J. Am. Chem. Soc.* **2009**, 131, 3846. (d) Boisvert, L.; Denney, M. C.; Kloek, H. S.; Goldberg, K. I. *J. Am. Chem. Soc.* **2009**, 131, 15802. (e) Zhu, M.-K.; Zhao, J.-F.; Loh, T.-P. *J. Am. Chem. Soc.* **2010**, 132, 6284. (f) Vedernikov, A. N. *Acc. Chem. Res.* **2012**, 45, 803.
- (3) Chuang, G. J.; Wang, W.; Lee, E.; Ritter, T. *J. Am. Chem. Soc.* **2011**, 133, 1760.
- (4) Khusnutdinova, J. R.; Rath, N. P.; Mirica, L. M. *J. Am. Chem. Soc.* **2012**, 134, 2414.
- (5) Khusnutdinova, J. R.; Qu, F.; Zhang, Y.; Rath, N. P.; Mirica, L. M. *Organometallics* **2012**, 31, 4627.
- (6) Bottino, F.; Di Grazia, M.; Finocchiaro, P.; Fronczek, F. R.; Mamo, A.; Pappalardo, S. *J. Org. Chem.* **1988**, 53, 3521.
- (7) Khusnutdinova, J. R.; Rath, N. P.; Mirica, L. M. *J. Am. Chem. Soc.* **2010**, 132, 7303.
- (8) See Supporting Information.
- (9) SADABS; Bruker Analytical X-Ray; Madison, WI, 2008.
- (10) Sheldrick, G. M. *Acta Crystallogr. Sect. A: Found. Crystallogr.* **2007**, 64, 112.
- (11) We have recently employed the Me_4N ligand to stabilize a series of Pd^{III} and Pd^{IV} complexes: Tang, F.; Qu, F.; Khusnutdinova, J. R.; Rath, N. P.; Mirica, L. M., submitted for publication in *Chem. Sci.*
- (12) A small amount of methane forms during aerobic oxidation, likely due to ligand decomposition from the Pd^{II} precursor or the Pd^{II} product (see Supporting Information). The mechanism of ligand decomposition is currently under investigation.
- (13) (a) Byers, P. K.; Canty, A. J.; Skelton, B. W.; White, A. H. *J. Chem. Soc., Chem. Commun.* **1986**, 1722. (b) Byers, P. K.; Canty, A. J.; Skelton, B. W.; White, A. H. *J. Chem. Soc., Chem. Commun.* **1987**, 1093. (c) Byers, P. K.; Canty, A. J.; Skelton, B. W.; White, A. H. *Organometallics* **1990**, 9, 826. (d) Canty, A. J.; Honeyman, R. T.; Roberts, A. S.; Traill, P. R.; Colton, R.; Skelton, B. W.; White, A. H. *J. Organomet. Chem.* **1994**, 471, C8. (e) Canty, A. J.; Jin, H.; Roberts, A. S.; Skelton, B. W.; Traill, P. R.; White, A. H. *Organometallics* **1995**, 14, 199. (f) Canty, A. J.; Dedieu, A.; Jin, H.; Milet, A.; Skelton, B. W.; Trofimenko, S.; White, A. H. *Inorg. Chim. Acta* **1999**, 287, 27. (g) Bayler, A.; Canty, A. J.; Edwards, P. G.; Skelton, B. W.; White, A. H. *J. Chem. Soc., Dalton Trans.* **2000**, 3325.
- (14) Byers, P. K.; Canty, A. J.; Crespo, M.; Puddephatt, R. J.; Scott, J. D. *Organometallics* **1988**, 7, 1363.
- (15) The additional peaks around the *m/z* value of 405 are tentatively assigned to [(Me_4N)PdO₂-H]⁺ (calcd 405.0543), which is likely a product of ligand oxidation and/or Pd^{II} product decomposition. The Me_4N ligand is flexible even when bonded to the Pd center and contains benzylic C–H bonds; thus it can undergo oxidation and ligand decomposition, as suggested by the less-than-quantitative yield of ligand-containing products at the end of the aerobic reactions. However, the formation of the Pd^{III} and Pd^{IV} species occurs much faster than any potential ligand oxidation/decomposition reactions, which are thus not responsible for the observed aerobic oxidation of the Pd^{II} center and the subsequent C–C bond formation. The ligand decomposition most likely occurs from the Pd^{II}-monomethyl products (see page S7 in the Supporting Information). A detailed characterization of the reaction side products is currently under way.

(16) (a) Rostovtsev, V. V.; Henling, L. M.; Labinger, J. A.; Bercaw, J. E. *Inorg. Chem.* **2002**, *41*, 3608. (b) Prokopchuk, E. M.; Jenkins, H. A.; Puddephatt, R. J. *Organometallics* **1999**, *18*, 2861. (c) Prokopchuk, E. M.; Puddephatt, R. J. *Can. J. Chem.* **2003**, *81*, 476.

(17) (a) Vedernikov, A. N.; Binfield, S. A.; Zavaliy, P. Y.; Khusnutdinova, J. R. *J. Am. Chem. Soc.* **2006**, *128*, 82. (b) Vedernikov, A. N. *Chem. Commun.* **2009**, 4781.

(18) Wieghardt, K.; Koeppen, M.; Swiridoff, W.; Weiss, J. *J. Chem. Soc., Dalton Trans.* **1983**, 1869.

(19) (a) Lanci, M. P.; Remy, M. S.; Kaminsky, W.; Mayer, J. M.; Sanford, M. S. *J. Am. Chem. Soc.* **2009**, *131*, 15618. (b) Seligson, A. L.; Trogler, W. C. *J. Am. Chem. Soc.* **1992**, *114*, 7085. (c) Johansson, L.; Ryan, O. B.; Romming, C.; Tilset, M. *Organometallics* **1998**, *17*, 3957.

(20) (a) Aye, T.-K.; Canty, A. J.; Crespo, M.; Puddephatt, R. J.; Scott, J. D.; Watson, A. A. *Organometallics* **1989**, *8*, 1518. (b) Markies, B. A.; Canty, A. J.; Boersma, J.; van Koten, G. *Organometallics* **1994**, *13*, 2053.